Acta Oceanol. Sin., 2022, Vol. 41, No. 2, P. 147–155
https://doi.org/10.1007/s13131-021-1769-3
http://www.aosocean.com
E-mail: ocean2@hyxb.org.cn

The influences of environmental factors on the air-sea coupling coefficient

Yanmin Zhang[1], Yifan Wang[1], Yunhua Wang[1, 2*], Yining Bai[1], Chaofang Zhao[1, 2]

[1] College of Information Science and Engineering, Ocean University of China, Qingdao 266100, China

[2] Laboratory for Regional Oceanography and Numerical Modeling, Pilot National Laboratory for Marine Science and Technology (Qingdao), Qingdao 266237, China

Received 18 September 2020; accepted 20 December 2020

Abstract

The response relationship between equivalent neutral wind speed anomaly (ENWSA) and sea-air temperature difference anomaly (SATDA) has been analyzed over four typical sea regions, i.e., the Kuroshio Extension, the Gulf Stream, the Brazil-Malvinas Confluence and the Agulhas Return Current. The results show that ENWSA is more sensitive to SATDA than sea surface temperature anomaly (SSTA), which implies that SATDA seems to be a more suitable parameter than SSTA to analyze the mesoscale air-sea interactions. Here, the slope of the linear relation between ENWSA and SATDA is defined as the air-sea coupling coefficient. It is found that the values of the coupling coefficient over the four typical sea areas have obvious seasonal variations and geographical differences. In order to reveal the reason of the seasonal variation and geographical difference of the coupling coefficient, the influences of some environmental background factors, such as the spatially averaged sea surface temperature (SST), the spatially averaged air temperature, the spatially averaged sea-air temperature difference and the spatially averaged equivalent neutral wind speed, on the coupling coefficient are discussed in detail. The results reveal that the background sea-air temperature difference is an important environmental factor which directly affects the magnitude of the coupling coefficients, meanwhile, the seasonal and geographical variations of the coupling coefficient.

Key words: air-sea coupling coefficient, SST, equivalent neutral wind speed, sea-air temperature difference

Citation: Zhang Yanmin, Wang Yifan, Wang Yunhua, Bai Yining, Zhao Chaofang. 2022. The influences of environmental factors on the air-sea coupling coefficient. Acta Oceanologica Sinica, 41(2): 147–155, doi: 10.1007/s13131-021-1769-3

1 Introduction

On a broad ocean basin scale, the correlation between sea surface temperature and sea surface wind speed is negative, which is indicative of an atmospheric forcing on the ocean (Namias and Cayan, 1981; Wallace et al., 1990; Liu et al., 1994; Mantua et al., 1997; Okumura et al., 2001). In recent years, mesoscale air-sea interaction has received much attention due to high resolution satellite measurements (Chelton and Xie, 2010; Xie, 2004). On medium spatial scales of 100–1 000 km near ocean fronts, however, positive correlation between ENWSA and SSTA is proved by satellite measurements, which indicates ocean-to-atmosphere forcing (Chelton and Xie, 2010; O'Neill, 2012; Liu et al., 2000; Chelton et al., 2001). Based on the satellite measurements, this positive correlation can be clearly found in different sea regions, such as the eastern tropical Pacific (Liu et al., 2000; Xie et al., 1998), the Arabian Sea (Vecchi et al., 2004), the Kuroshi (Nonaka and Xie, 2003; Liu and Xie, 2008; Xu et al., 2010), the Gulf Stream (GS) (Xie, 2004; Chelton et al., 2004; Park and Cornillon, 2002; Park et al., 2006), the Brazil-Malvinas Confluence (BMC) (Tokinaga et al., 2005; Pezzi et al., 2005) and the Agulhas Return Current (ARC) (O'Neill et al., 2005, 2010; Liu et al., 2007; Song et al., 2009). This positive correlation between equivalent neutral wind speed anomaly (ENWSA) and sea surface temperature anomaly (SSTA) is also supported by *in-situ* observations and the results of numerical model (Small et al., 2003; Maloney and Chelton, 2006).

The influence of mesoscale sea surface temperature (SST) on the atmosphere has been investigated in a number of studies. O'Neill et al. (2010) defined the slope of the linear relation between ENWSA and SSTA as the air-sea coupling coefficient. Using satellite wind field and SST measurements from June 2002 to August 2008, O'Neill et al. estimated value of the coupling coefficient over four mid-latitude SST frontal zones, i.e., the Kuroshio Extension, the Gulf Stream, the Brazil-Malvinas Confluence and the Agulhas Return Current regions. They found that the coupling coefficients between ENWSA and SSTA are variant in these regions, and their values are generally higher over the Southern Hemisphere than those over the Northern Hemisphere. However, the reasons leading to the geographical differences in the coupling coefficients still need to be further analyzed.

In the previous studies, more attentions were paid to the response relationship between ENWSA and SSTA. However, according to the similarity theory of Monin et al. (1971), the equivalent neutral wind speed (ENWS) is mainly related to atmospheric stability (i.e., sea-air temperature difference) rather than SST. Therefore, the investigation on the response relationship

Foundation item: The National Key Research and Development Program of China under contract No. 2016YFC1401008; the National Natural Science Foundation of China under contract Nos 41976167 and 41576170; the National Natural Science Foundation of China-Shandong Joint Fund for Marine Science Research Centers under contract No. U1606404.
*Corresponding author, E-mail: yunhuawang@ouc.edu.cn

between equivalent neutral wind speed and sea-air temperature difference is likely more conducive to revealing the essence of the sea-air coupling characteristics. In the present work, the response relationship between ENWSA and SATDA has been analyzed utilizing the monthly average equivalent neutral wind speed and sea-air temperature difference over the four typical sea regions. Similar to the coupling coefficient defined by O'Neill et al. (2010), the slope of the linear relation between ENWSA and SATDA is defined as the new air-sea coupling coefficient. Just as expected, over the four typical ocean regions, the value of the new coupling coefficient is obviously greater than the coupling coefficient defined by O'Neill et al. (2010). This result indicates that ENWSA is more sensitive to SATDA than SSTA. Furthermore, it is also found that the new coupling coefficient show obvious seasonal variations and geographical differences. In order to reveal the reason of the seasonal variation and geographical differences of the new coupling coefficient, the influences of some environmental background parameters, such as the SST, the air temperature, the sea-air temperature difference and the equivalent neutral wind speed, should be discussed in detail.

This paper is organized as follows: the satellite and the ECMWF data used in this work are introduced briefly in Section 2. The definition of the new coupling coefficient and its variation with season and sea region are presented in Section 3. In Section 4, theoretical analysis of the effects of environment parameters on the new coupling coefficient is carried out by the Monin similarity principle. In Section 5, based on the satellite and the ECMWF data, the correlations between the background SST, the background air temperature, the background equivalent neutral wind speed and the background sea-air temperature difference with the new coupling coefficient are discussed in detail. And the summary of this paper is drawn in the final section.

2 The data used in this work

The mesoscale air-sea interaction characteristics above four typical sea areas including KE, ARC, GS, and BMC have been studied by Maloney and Chelton (2006). The locations of these four areas are shown in Fig. 1.

In this work, the wind fields and the SST acquired respectively by the advanced scatterometer (ASCAT) and the WindSat polarimetric radiometer from January 2008 to December 2017 are used to investigate the mesoscale air-sea interaction over the four typical sea areas. The spatial resolution of the wind field and the SST is 0.25° by 0.25° along longitude and latitude directions. The previous studies indicated that the persistence of ocean-atmosphere coupling near mid-latitude fronts is strongest on timescales of a few weeks to months (O'Neill et al., 2005; Chelton et al., 2007). Therefore, in our work, the monthly grid wind fields and SST are selected. Here, the monthly-averaged air temperature field of the ECMWF at 2 m above ocean surface is used as the atmospheric temperature, and the spatial resolution of air temperature is the same with the wind field and the SST. In our study, the spatial anomaly SSTA, air temperature anomaly, ENWSA and SATDA fields are all obtained by high pass filtering with a sliding window size 4°×4° along longitude and latitude directions. In addition, the wind fields and the SST acquired by QSCAT and AMSR-E from June 2002 to November 2009 are also used to further confirm the conclusions obtained based on the data acquired by the ASCAT and the WindSat from January 2008 to December 2017.

The wind field data (ASCAT, QuikSCAT) and the SST data (AMSR-E, WindSat) are downloaded from the website: http://www.remss.com. The monthly-averaged air temperature field of the ECMWF are downloaded from the website: https://cds.climate.copernicus.eu/cdsapp#!/ dataset/reanalysis-era5-single-levels?tab=form.

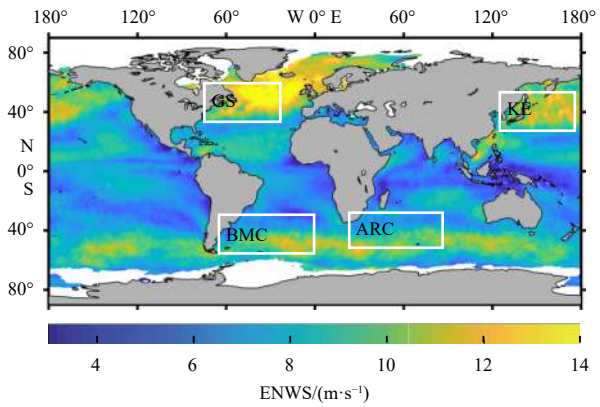

Fig. 1. Four typical sea areas for studying in this paper. The map is the monthly-averaged equivalent neutral wind speed (ENWS) acquired by the advanced scatterometer in August 2013. GS. the Gulf Stream; KE. the Kuroshio Extension; BMC. the Brazil-Malvinas Confluence; ARC. the Agulhas Return Current.

3 The response relationship between ENWSA and SATDA

In the previous papers, the response relationship between ENWSA and SSTA has been discussed many times. The linear relationship between ENWSA and SSTA, i.e. the slope of the least squares fitting line, is defined as the coupling coefficient, which can be expressed as (O'Neill et al., 2010)

$$k_{\mathrm{SSTA}} = \mathrm{ENWSA}/\mathrm{SSTA}. \tag{1}$$

However, the similarity principle of Monin et al. (1971) implies that the sea-air temperature difference affects the equivalent neutral wind speed more directly than the SST. Thus, in the present work, the linear response of ENWSA to SATDA is defined as a new coupling coefficient to reflect the strength of air-sea interaction. The new coupling coefficient can be expressed as

$$k_{\mathrm{SATDA}} = \mathrm{ENWSA}/\mathrm{SATDA}. \tag{2}$$

As an example, the map of the ENWSA (colors) and SSTA (contours) fields in December 2010 over the Agulhas Return Current region is shown in Fig. 2a, and the corresponding scatter plot is presented in Fig. 2b. From Fig. 2a, one can find that the ENWSA is positively correlated with the SSTA, i.e. the higher (lower) wind speed is over the warmer (colder) water. The scatter plot shows that the correlation coefficient between the ENWSA and the SSTA is 0.69 and the least squares fitting slope k_{SSTA} is 0.44. For comparison, the map of the ENWSA (colors) and the SATDA (contours) fields in December 2010 over the Agulhas Return Current region is shown in Fig. 2c and the corresponding scatter plot is presented in Fig. 2d. The results in Figs 2c and d show that the ENWSA is also positively correlated with the SATDA and the scatter plot is very similar with that shown in Fig. 2b. However, the value of new coupling coefficient k_{SATDA} ($k_{\mathrm{SATDA}} = 0.57$) is obvious higher than k_{SSTA}.

In order to show the difference between the coupling coefficients k_{SATDA} and k_{SSTA} more clearly, the values of these two parameters over the four typical regions are presented in Fig. 3. Here, the values of k_{SATDA} and k_{SSTA} have been smoothed with a moving-average filter and the filtering window is 3. Firstly, the curves

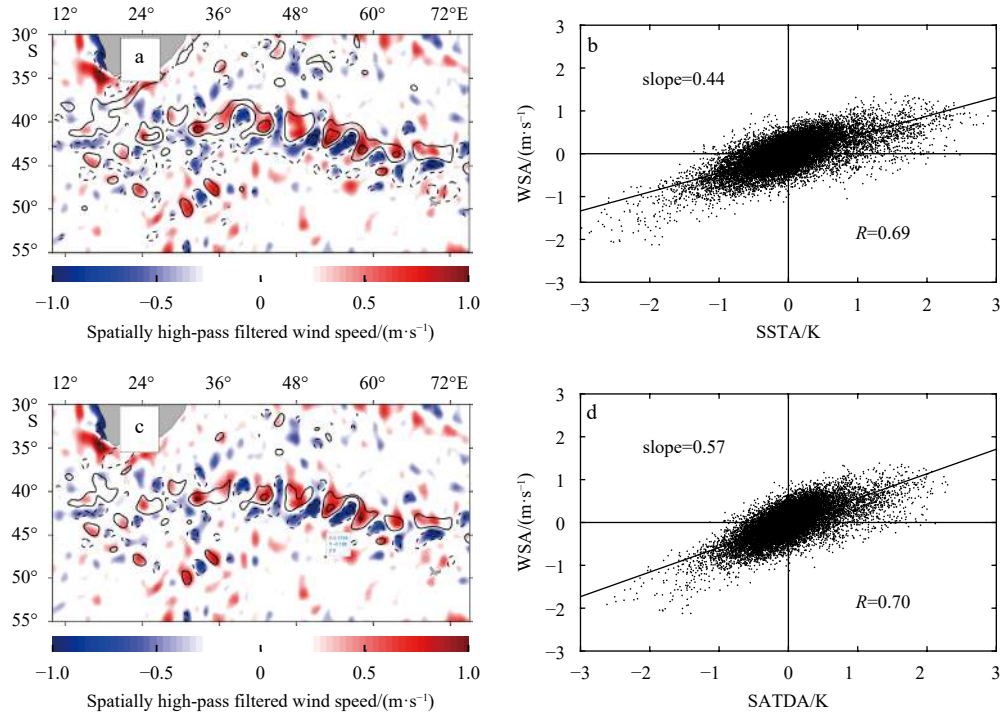

Fig. 2. The map of sea surface temperature anomaly (SSTA) overlaid as contours on equivalent neutral wind speed anomaly (ENWSA) at the Agulhas Return Current region in December 2010 (a), and the corresponding scatter plot (b); the map of sea-air temperature difference anomaly (SATDA) overlaid as contours on ENWSA (c), and the corresponding scatter plot (d). The parameter R in b and d denotes the correlation coefficient, and the solid thick line is the linear least square fitting line to the points. WSA. wind speed anomaly.

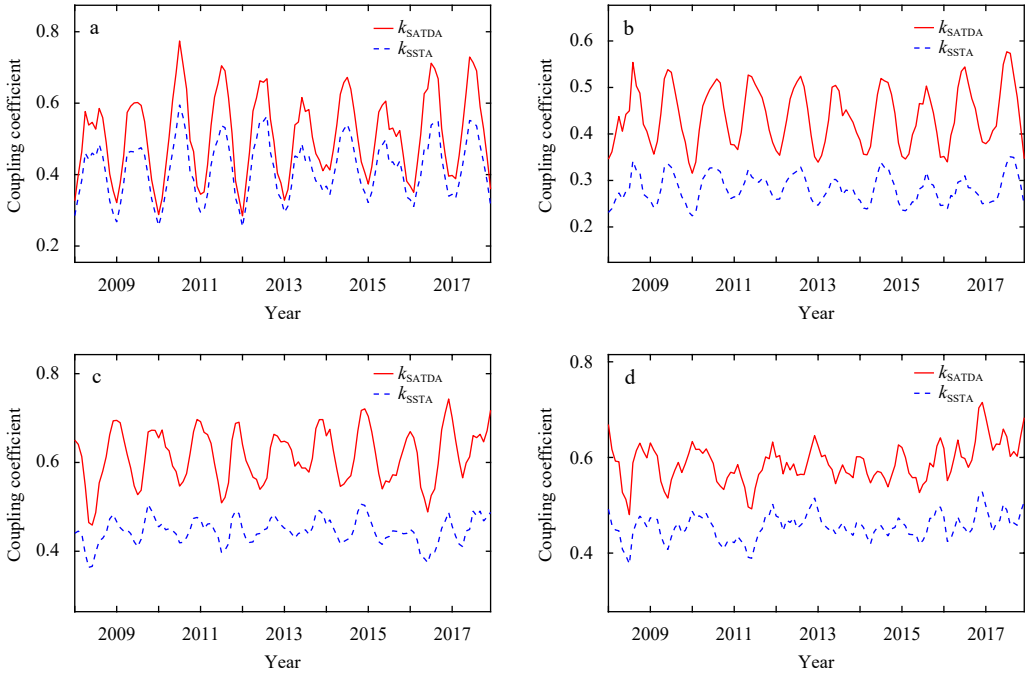

Fig. 3. The values of the k_{SSTA} (blue dashed curves) and k_{SATDA} (red solid curves) from January 2008 to December 2017 over the four typical regions, i.e. the Kuroshio Extension (a), the Gulf Stream (b), the Brazil-Malvinas Confluence (c) and the Agulhas Return Current (d) region.

in Fig. 3 show that k_{SATDA} and k_{SSTA} are both varying with season and the variation tendencies of them are similar with each other. Over the Kuroshio Extension and the Gulf Stream, k_{SATDA} and k_{SSTA} generally reach the maximum values in July or August, while the minimum values occur in December or January. On the contrary, over the Brazil-Malvinas Confluence and the Agulhas Return Current regions, the maximum values of the coupling coefficients occur in December or January, while the minimum

values occur in July or August. In short, the coupling coefficient reaches its maximum (minimum) value in summer (winter). Secondly, it is also found that the coupling coefficients have obvious geographic differences. Over the Kuroshio Extension, the Gulf Stream, the Brazil-Malvinas Confluence and the Agulhas Return Current regions, the mean values of k_{SATDA} are 0.47, 0.45, 0.57 and 0.59, and the mean values of k_{SSTA} are 0.37, 0.31, 0.41 and 0.46, respectively. The results show that the values of k_{SATDA} and k_{SSTA} are much larger in the two Southern Hemisphere regions than those in the two Northern Hemisphere regions. O'Neill et al. (2010) pointed out that the geographical differences in the coupling coefficients between the four regions are likely due to geographic differences in the vertical structure of the boundary layer and large-scale forcing. However, the question of which environmental parameters cause the geographical differences of the coupling coefficients still needs in-depth analysis. The results in Fig. 3 show that the values of k_{SATDA} over the four regions are obvious larger than k_{SSTA}, which implies that ENWSA is more sensitive to SATDA than SSTA. This conclusion is consistent with the similarity principle of Monin et al. (1971), and therefore the new coupling coefficient k_{SATDA} seems to be more suitable to describe the sea-air coupling characteristics. Thus, in the following discussion, k_{SATDA} is taken as the coupling coefficient instead of k_{SSTA}.

The value of coupling coefficient reflects the strength of sea-air coupling. The results in Fig. 3 show that the coupling coefficient k_{SATDA} has obvious seasonal and geographic variations over the four typical sea areas. To better understand the reasons of the seasonal variations and the geographic differences, in the following sections, the effects of various environmental parameters on k_{SATDA} are discussed in detail.

4 Theoretical analysis on the effects of environment parameters

Firstly, the theoretical expression of the wind speed profile is introduced in brief for better understanding the response of ENWS to environment parameters. Considering the atmospheric stratification effect, based on the similarity principle of Monin et al. (1971), the wind speed profile is expressed by

$$u_z = \frac{u_{\mathrm{f}}}{\kappa}\left(\ln\frac{z}{z_0} - \Phi\right), \tag{3}$$

where z is the height above sea surface. Here, it is set z=10 m. u_{f} is the friction wind speed. κ=0.41 is the Karman constant. z_0 is the roughness length. Φ denotes the atmospheric stratification function (Large and Pond, 1981),

$$\Phi = \begin{cases} -5z/L, & z/L \geqslant 0, \\ 2\ln\left[(1+x)/2\right] + \ln\left[\left(1+x^2\right)/2\right] - \\ 2\tan^{-1}x + \pi/2, & z/L < 0, \end{cases} \tag{4}$$

where $x = (1-16z/L)^{1/4}$, L is the Monin-Obukhov length, the ratio z/L is proportional to the Richard number Ri, and can be expressed as

$$z/L = \kappa C_T C_d{}^{-3/2} Ri(\Delta T), \tag{5}$$

$C_T \approx 1.0\times10^{-3}$ and $C_d \approx 1.25\times10^{-3}$ are empirical parameters, the Richard number is

$$Ri(\Delta T) = -\frac{gz\Delta T}{u_z{}^2 T_0}\left(1 + T_0^2\frac{\Delta Q}{\Delta T}\times 1.72\times10^{-6}\right), \tag{6}$$

g = 9.81 m/s^2 is the gravitational acceleration constant, $\Delta T = T_{\mathrm{w}} - T_{\mathrm{a}}$ denotes the sea-air temperature difference, T_{w} and T_{a} denote the temperatures of the water and air in Kelvin. T_0 is the average temperature of T_{a},

$$\Delta Q = 6.404\times10^8\left[0.98\exp\left(-\frac{5\,107}{T_{\mathrm{w}}}\right) - 0.75\exp\left(-\frac{5\,107}{T_{\mathrm{a}}}\right)\right]. \tag{7}$$

Under neutrally stratified condition (i.e. $\Delta T = 0$ K), the wind speed profile is as follows:

$$u_{\mathrm{zn}} = \frac{u_{\mathrm{f}}}{\kappa}\left(\ln\frac{z}{z_0}\right). \tag{8}$$

Substituting Eq. (8) into Eq. (3), the ENWS is obtained as

$$u_{\mathrm{zn}} = u_z + \frac{u_{\mathrm{f}}}{\kappa}\Phi, \tag{9}$$

where the friction velocity u_{f} is related to the drag coefficient by

$$u_{\mathrm{f}} = \sqrt{C_{dzn}}u_{\mathrm{zn}}, \tag{10}$$

the drag coefficient can be evaluated by (Wu, 1980)

$$C_{dzn} = (0.8 + 0.065u_{\mathrm{zn}})\times10^{-3}. \tag{11}$$

From Eq. (9), the first-order derivative of the ENWS to the air-sea temperature difference is obtained as follows

$$\frac{\mathrm{d}u_{\mathrm{zn}}}{\mathrm{d}\Delta T} = \frac{1}{\kappa}\left[\frac{\mathrm{d}u_{\mathrm{f}}}{\mathrm{d}\Delta T}\Phi + u_{\mathrm{f}}\frac{\mathrm{d}\Phi}{\mathrm{d}\Delta T}\right]. \tag{12}$$

The expressions of the derivatives $\frac{\mathrm{d}u_{\mathrm{f}}}{\mathrm{d}\Delta T}$ and $\frac{\mathrm{d}\Phi}{\mathrm{d}\Delta T}$ are as following (Wang et al., 2014)

$$\frac{\mathrm{d}u_{\mathrm{f}}}{\mathrm{d}\Delta T} = \left[\frac{\kappa u_z}{2(\kappa\sqrt{C_{dzn}} - C_{dzn}\Phi)} + \frac{\kappa u_z\Phi}{2(\kappa - \sqrt{C_{dzn}}\Phi)^2}\right]\frac{\mathrm{d}C_{dzn}}{\mathrm{d}\Delta T} + \frac{\kappa C_{dzn}u_z}{(\kappa - \sqrt{C_{dzn}}\Phi)^2}\frac{\mathrm{d}\Phi}{\mathrm{d}\Delta T}, \tag{13}$$

$$\frac{\mathrm{d}\Phi}{\mathrm{d}\Delta T} = \begin{cases} \dfrac{28.4\kappa C_T C_d^{-3/2}}{(1-16z/L)^{3/4}u_{10}^2}\dfrac{2a^2}{(1+a)(1+a^2)}, & z/L < 0 \ \text{unstable}, \\ 17.75\dfrac{\kappa C_T C_D^{-3/2}}{u_{10}^2}, & z/L \geqslant 0 \ \text{stable}, \end{cases} \tag{14}$$

$$\frac{\mathrm{d}C_{dzn}}{\mathrm{d}\Delta T} \approx 0.475\times10^{-3}\alpha^{1/2}\frac{1}{\kappa}\left[\frac{\kappa C_{dzn}u_z}{(\kappa - \sqrt{C_{dzn}}\Phi)^2}\Phi + u_{\mathrm{f}}\right]\frac{\mathrm{d}\Phi}{\mathrm{d}\Delta T}. \tag{15}$$

In general, because SATDA in Eq. (2) is small, thus the coupling coefficient k_{SATDA} is approximately equal to $\mathrm{d}u_{\mathrm{zn}}/\mathrm{d}\Delta T$, i.e.

$$k_{\mathrm{SATDA}} \approx \frac{\mathrm{d}u_{\mathrm{zn}}}{\mathrm{d}\Delta T}. \tag{16}$$

Therefore, the first-order derivative of the equivalent neutral wind speed to the air-sea temperature difference (i.e. $\frac{\mathrm{d}u_{\mathrm{zn}}}{\mathrm{d}\Delta T}$) can be considered as the theoretical coupling coefficient.

The ENWS evaluated based on the similarity principle of Monin and the corresponding coupling coefficient (i.e. the first-order derivative) are presented in Figs 4a and b, respectively. Here, the water temperature T_w is set to be 293 K. The curves in Fig. 4 show that ENWS increases with SATD for different wind speed. If the sea-air temperature difference $\Delta T \leqslant 0$ K, the value of the coupling coefficient increases with SATD. On the contrary, if the sea-air temperature difference $\Delta T > 0$ K, the value of the coupling coefficient decreases with the increasing of SATD. From the results, it is concluded that the response of ENWS and SATD is the most sensitive under neutrally stratified condition. As shown in Fig. 4, wind speed also has an effect on the coupling coefficient. If the sea-air temperature difference is within $[-7\text{ K}, 0.5\text{ K}]$, the value of the coupling coefficient decreases with the increase of wind speed; otherwise, it increases with wind speed. However, under unstable atmospheric condition (i.e. $\Delta T > 0$ K), it should be pointed out that the effect of wind speed on the coupling coefficient is not obvious.

In addition to the air-sea temperature difference and wind speed, the effects of the water temperature T_w and the air temperature T_a on the coupling coefficient are shown in Fig. 5. In Fig. 5a, the air temperature is set to be 290 K. In Fig. 5b, the water temperature is equal to 290 K. From the curves it is found that the effects of T_w and T_a on the coupling coefficient are both negligible.

5 Analysis based on the satellite measured data

From the theoretical analysis in the previous section, it is found that the sea-air temperature difference is the most important factor affecting the coupling coefficient. Under unstable atmospheric condition, the effects of SST, equivalent neutral wind speed and air temperature on the coupling coefficient are not obvious, and even can be neglected. In order to further prove this conclusion, in this section, the effect of the environment parameters on the coupling coefficient are also analyzed based on the satellite measurement and the ECMWF reanalysis air temperature data.

As an example, the curves of RMMSST, RMMWS, RMMAT and RMMSATD in the Brazil Malvinas Confluence region vary with season are shown in Figs 6a–d. Here, RMMSST, RMMWS, RMMAT and RMMSATD denote the values of the spatially averaged SST, spatially averaged equivalent neutral wind speed, spatially averaged air temperature and spatially averaged sea-air temperature difference over the Brazil Malvinas Confluence region and can be considered as the background environment parameters. The corresponding scatter plots of the coupling coefficient and the environment parameters are shown in Figs 6e–h. From Fig. 6, it is found that there are correlations between the coupling coefficient and the background environment parameters. In our work, the statistic correlation coefficients between the coupling coefficient and the background environment parameters in the other three typical sea areas are also evaluated and the results are given in Table 1. The results in Table 1 also imply that these four environment parameters all have obvious effects on the coupling coefficient. As can be seen from Fig. 6d, the average sea-air temperature difference in different months is greater than 0 K. This means that the sea-air boundary layer over the Brazil-Malvinas Confluence region is under an unstable state. Accord-

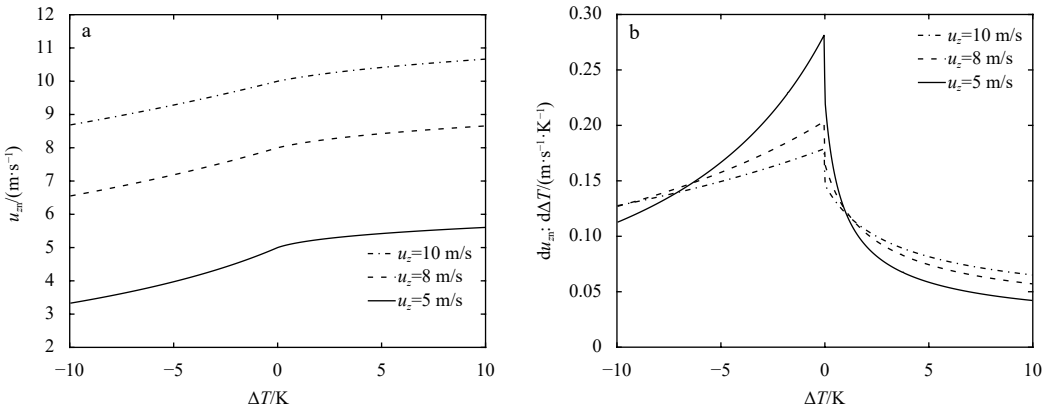

Fig. 4. The ENWS evaluated by Eq. (9) (a) and the coupling coefficient evaluated by Eq. (16) (b) as functions of the sea-air temperature difference ΔT.

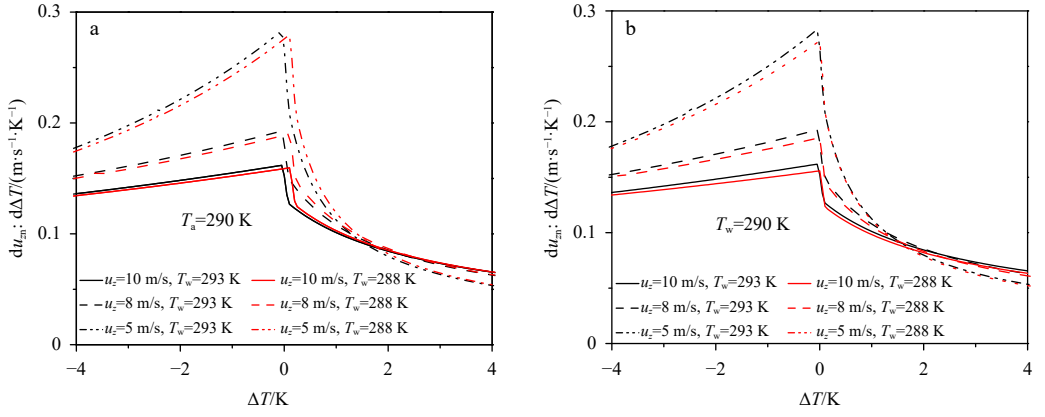

Fig. 5. The coupling coefficient as functions of ΔT for different T_w and T_a are presented in a and b, respectively.

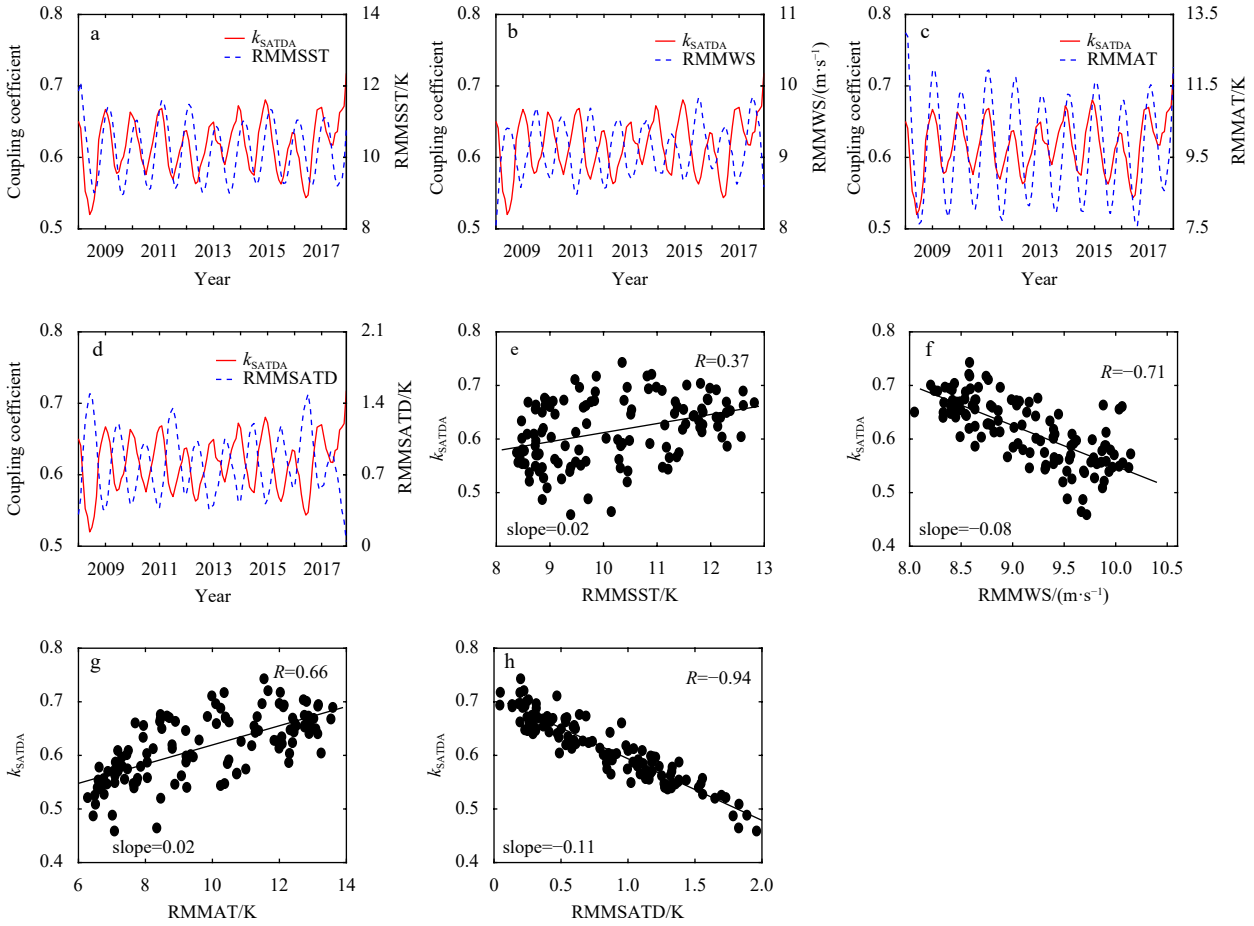

Fig. 6. The values of the coupling coefficient (red solid curve) and RMMSST, RMMWS, RMMAT and RMMSATD (blue dashed curve) from January 2008 to December 2017 over the Brazil-Malvinas Confluence region (a–d), and the corresponding scatter plots (e–h). The parameter *R* denotes the correlation coefficient.

Table 1. The correlation coefficients between coupling coefficient and the environment parameters over the four areas

Sea area	Environment parameters	Correlation coefficient	Sea area	Environment parameters	Correlation coefficient
KE	RMMSST	0.43	BMC	RMMSST	0.37
	RMMWS	−0.88		RMMWS	−0.71
	RMMAT	0.65		RMMAT	0.66
	RMMSATD	−0.93		RMMSATD	−0.94
GS	RMMSST	0.76	ARC	RMMSST	0.45
	RMMWS	−0.83		RMMWS	−0.62
	RMMAT	0.87		RMMAT	0.55
	RMMSATD	−0.89		RMMSATD	−0.86

ing to the theoretical results in Section 4, under unstable atmospheric condition, the effects of SST, ENWS and AT on the coupling coefficient are not obvious, and even can be neglected. Obviously, the conclusion obtained based on the satellite data is not consistent with the theoretical results. What causes this inconsistency? Further analysis of the relationship between the four environmental parameters shows that there are obvious cross-correlation between each of them, such as RMMSATD is negatively correlated with RMMSST and RMMAT, and positively correlated with RMMWS (see the cross-correlation coefficient in Table 2). Just because of the cross correlations between these four environmental parameters, it is difficult to determine which parameter is the main factor affecting the coupling coefficient.

To further analyze which parameter is the main factor affecting the coupling coefficient, in Fig. 7, the scatter plots of the coupling coefficient varying with the environment parameter over the four regions are plotted together. In Figs 7a–d, the dash line denotes the fitting line based on the overall data of the four regions. As shown in Figs 7a and c, the slopes of the fitting lines are both negative, i.e. the coupling coefficient decreases with RMMSST and RMMAT. However, the scatter plot indicates that the coupling coefficient is positively related to RMMSST and RM-

Table 2. The cross-correlation coefficients between the four environment parameters

	RMMSST	RMMWS	RMMAT	RMMSATD
RMMSST	1	−0.66	0.97	−0.51
RMMWS	−0.66	1	−0.79	0.85
RMMAT	0.97	−0.79	1	−0.70
RMMSATD	−0.51	0.85	−0.70	1

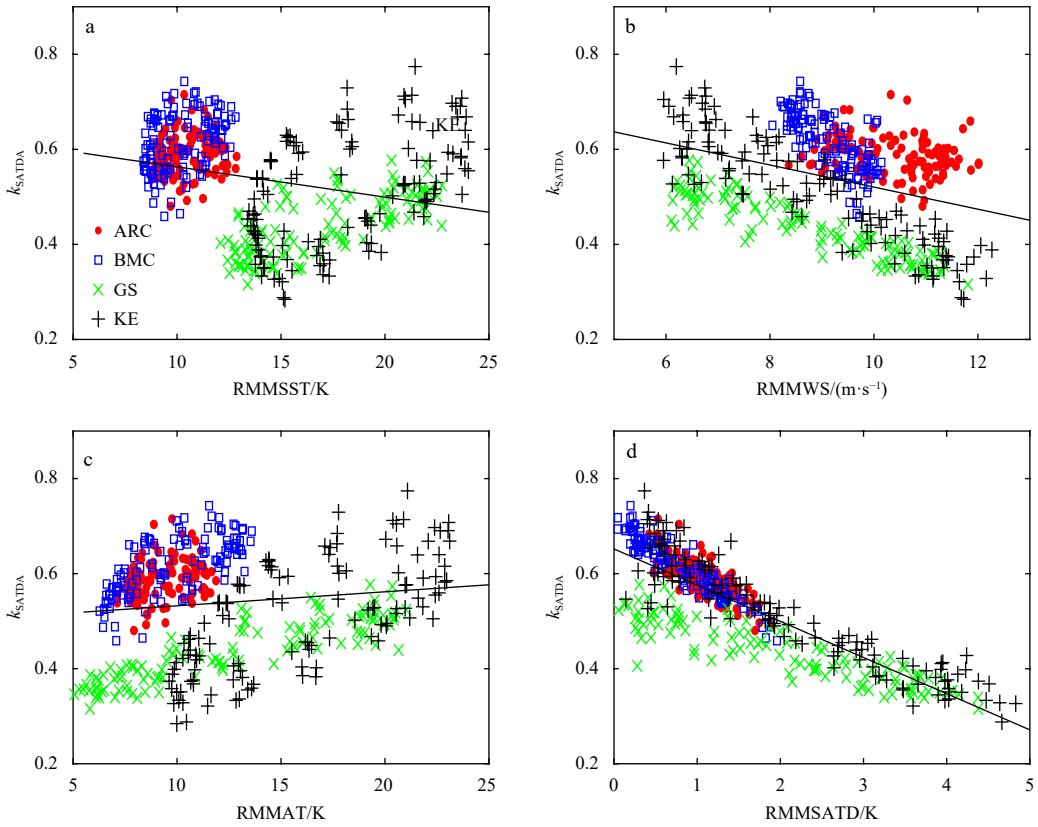

Fig. 7. The scatter plots of the background environmental parameters and the coupling coefficient over the four sea regions. The red solid circles, the green asterisks, the blue squares and the black pluses represent the data in the Kuroshio Extension (KE), the Gulf Stream (GS), the Brazil-Malvinas Confluence (BMC) and the Agulhas Return Current (ARC) regions respectively.

MAT. This contradictory phenomenon means that RMMSST and RMMAT are both not the key environment parameters which affect the coupling coefficient. From the results in Fig. 7b, it is found that the fitting line shows that the coupling coefficient is negatively related to RMMWS, and the coupling coefficient in each sea region also decreases with RMMWS. However, the values of the coupling coefficient over the four regions are widely varying for a same RMMWS. Obviously, RMMWS is also not the key parameter that directly affects the coupling coefficient. The influence of RMMSATD on the coupling coefficient is shown in Fig. 7d. The results in Fig. 7d show that the slope of the fitting line based on the overall data are consistent with the trend of the scatter plot of each sea region. Unlike the results in Fig. 7b, for a same RMMSATD, the difference of the coupling coefficient among various sea area are not obvious. Through the above analysis, it is concluded that RMMSATD is the key environment parameter that directly affects the coupling coefficient. Despite the value difference of the coupling coefficient, this conclusion is consistent with the theoretical results obtained in Section 4.

In Fig. 8, the dashed line denotes the linear fitting line (LFL) and its expression is

$$k_{\mathrm{SATDA}} = \alpha \cdot \langle \Delta T \rangle + \beta, \tag{17}$$

with $\alpha = -0.110\,6$ and $\beta = 0.710\,4$. $\langle \Delta T \rangle$ denotes the RMMSATD. The solid line is the nonlinear fitting line (NLFL) and its expression can be expressed as

$$k_{\mathrm{SATDA}} = A \cdot \langle \Delta T \rangle^2 + B \cdot \langle \Delta T \rangle + C, \tag{18}$$

with $A = 0.010\,3$, $B = -0.125\,3$ and $C = 0.708\,5$.

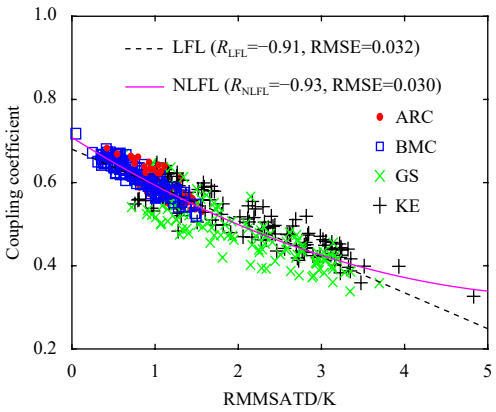

Fig. 8. The linear and the nonlinear relationships between RMMSATD and the coupling coefficient. The dashed and the solid lines denote the linear (LFL) and the nonlinear fitting lines (NLFL), respectively. R and RMSE denote the correlation coefficient and the root-mean-square error.

From Fig. 8, it is found that the nonlinear line fits the scatter data better than the linear line. The trend of the nonlinear line is more consistent with the theoretical result under unstable atmospheric condition. Since RMMSATD is the key environment parameter affecting the coupling coefficient, it is not surprising that the seasonal variation and geographic difference of the coupling coefficient would disappear or at least obviously decrease if the coupling coefficients in the four regions are calibrated to a same RMMSATD.

The modified coupling coefficients based on Eq. (18) can be expressed as

$$k_{\mathrm{m\_SATDA}}=k_{\mathrm{SATDA}}-[A\cdot(\langle\Delta T\rangle^2-\Delta T_u^2)+B\cdot(\langle\Delta T\rangle-\Delta T_{\mathrm{u}})], \quad (19)$$

where ΔT_{u} denotes the uniform RMMSATD constant and it is set to be 9 K in this work. The original coupling coefficient k_{SATDA} and the modified coupling coefficient $k_{\mathrm{m\_SATDA}}$ are presented in Fig. 9a and b, respectively. The curves in Fig. 9a show that the seasonal variations and geographic differences of the original coupling coefficient in the four sea regions are very remarkable. However, if the coupling coefficients in the four regions are calibrated to a same RMMSATD, compared with the original coupling coefficient in Fig. 9a, the seasonal variations and geographic differences of the modified coupling coefficient are no longer remarkable. In order to further prove this conclusion, the coupling coefficient and the modified coupling coefficient evaluated based on the other remote sensing data are presented in Fig. 10. Here, the wind filed and SST data were acquired by QSCAT and AMSR-E from June 2002 to November 2009. Although the wind field and SST data in Fig. 10 were acquired by the satellite sensors different from those in Fig. 9, the same conclusion can also be obtained from Fig. 10.

From what has been discussed above, a conclusion can be obtained that the seasonal variations and the geographic differences of the coupling coefficient in the four typical regions are caused by the changes of RMMSATD with season and region. There are pseudo-correlations between RMMSST, RMMWS, RMMAT with the coupling coefficient, the results are probably due to the cross-correlation between RMMSATD and the other three parameters.

6 Summary

The response relationship between sea surface equivalent neutral wind speed anomaly and sea-air temperature difference anomaly has been discussed over four typical sea regions and the influences of environment parameters, such as the background sea surface temperature, the background air temperature, the background wind speed and the background sea-air temperature difference on the coupling coefficient are also analyzed. The main contributions and conclusions of this work are as follows:

(1) The value of the new coupling coefficient k_{SATDA} is obvious larger than that of k_{SSTA}, which implies that the mesoscale wind speed anomaly is more sensitive to the sea-air temperature difference anomaly than that to SST anomaly. This new coupling coefficient is likely more suitable to indicate the intensity of air-sea coupling.

(2) The theoretical analysis based on the similarity principle of Monin reveals that the new coupling coefficient is mainly affected by SATD. Especially, under unstable atmospheric condition, the effects of ENWS, SST and air temperature (AT) even can be neglected.

(3) The satellite data shows that the value of k_{SATDA} is apparently to be correlated with RMMSST, RMMENWS, RMMAT and RMMSATD. However, a deep analysis shows that RMMSATD is the key environment parameter directly affecting the new coupling coefficient. The seasonal variations and the geographic dif-

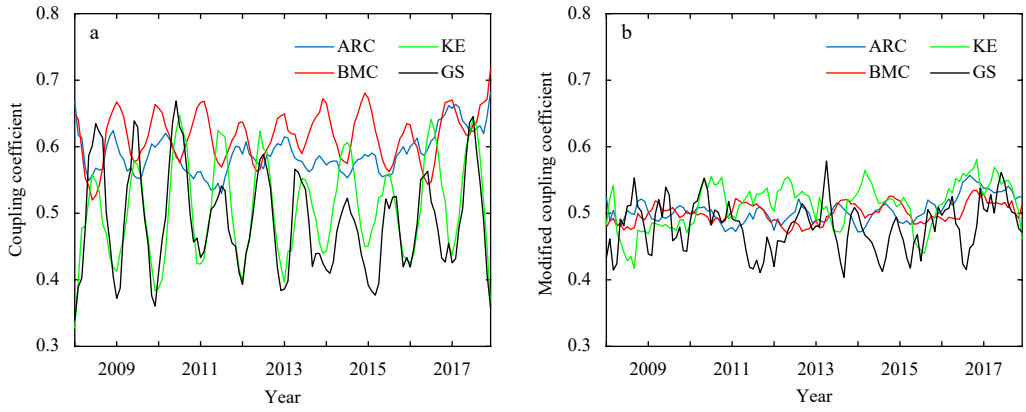

Fig. 9. The coupling coefficient (a) and the modified coupling coefficient (b) from January 2008 to December 2017 over the four regions.

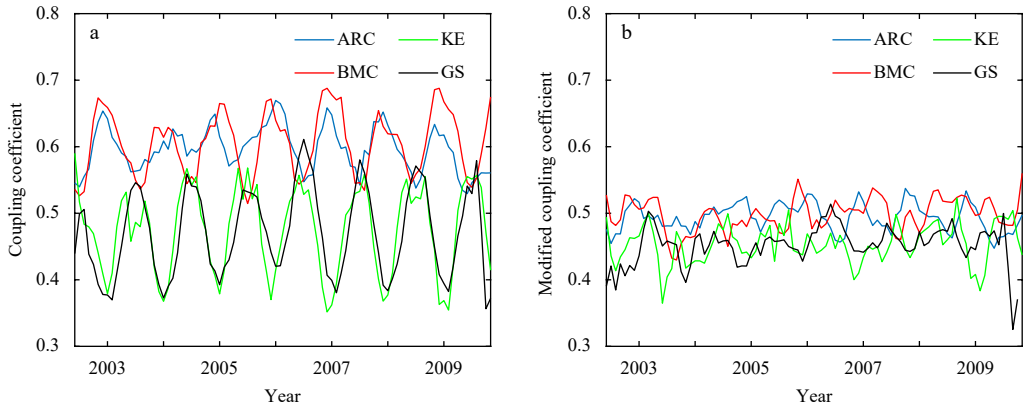

Fig. 10. The coupling coefficient (a) and the modified coupling coefficient (b) , the wind filed and SST data were acquired by QSCAT and AMSR-E from June 2002 to November 2009, respectively.

ferences of the new coupling coefficient in the four typical regions are caused by the changes of the background RMMSATD with season and region. The pseudo-correlations between the new coupling coefficient with RMMSST, RMMENWS, RMMAT, the results are probably due to the cross-correlations between RMMSATD and the other three environment parameters.

In this work, only the response relationship between the mesoscale equivalent neutral wind speed anomaly (ENWSA) and the mesoscale sea-air temperature difference anomaly (SATDA) has been analyzed over four typical sea regions. In fact, the divergence and curl of the sea surface wind filed would also be affected by SST gradient. The previous researches revealed that the divergence and the curl of the wind stress are related to the downwind- and the crosswind-component of the SST gradient respectively (O'Neill et al., 2003, 2005; Small et al., 2008). Because of the correlation between the SATD gradient and the SST gradient, it is expected that the divergence and the curl of the ENWS would also be affected by the SATD gradient. The relevant analysis and discussion will be carried out in our future work.

References

Chelton D B, Esbensen S K, Schlax M G, et al. 2001. Observations of coupling between surface wind stress and sea surface temperature in the eastern tropical Pacific. Journal of Climate, 14(7): 1479–1498, doi: 10.1175/1520-0442(2001)014<1479:OOCBSW>2.0.CO;2

Chelton D B, Schlax M G, Freilich M H, et al. 2004. Satellite measurements reveal persistent small-scale features in ocean winds. Science, 303(5660): 978–983, doi: 10.1126/science.1091901

Chelton D B, Schlax M G, Samelson R M. 2007. Summertime coupling between sea surface temperature and wind stress in the California Current System. Journal of Physical Oceanography, 37(3): 495–517, doi: 10.1175/JPO3025.1

Chelton D B, Xie Shangping. 2010. Coupled ocean-atmosphere interaction at oceanic mesoscales. Oceanography, 23(4): 52–69, doi: 10.5670/oceanog.2010.05

Large W G, Pond S. 1981. Open ocean momentum flux measurements in moderate to strong winds. Journal of Physical Oceanography, 11(3): 324–336, doi: 10.1175/1520-0485(1981)011<0324:OOMFMI>2.0.CO;2

Liu W T, Xie Xiaosu. 2008. Ocean-atmosphere momentum coupling in the Kuroshio Extension observed from space. Journal of Oceanography, 64(4): 631–637, doi: 10.1007/s10872-008-0053-x

Liu W T, Xie Xiaosu, Niiler P P. 2007. Ocean-atmosphere interaction over Agulhas Extension meanders. Journal of Climate, 20(23): 5784–5797, doi: 10.1175/2007JCLI1732.1

Liu W T, Xie Xiaosu, Polito P S, et al. 2000. Atmospheric manifestation of tropical instability wave observed by QuikSCAT and tropical rain measuring mission. Geophysical Research Letter, 27(16): 2545–2548, doi: 10.1029/2000GL011545

Liu W T, Zhang Anzhen, Bishop J K B. 1994. Evaporation and solar irradiance as regulators of sea surface temperature in annual and interannual changes. Journal of Geophysical Research: Oceans, 99(C6): 12623–12637, doi: 10.1029/94JC00604

Maloney E D, Chelton D B. 2006. An assessment of the sea surface temperature influence on surface wind stress in numerical weather prediction and climate models. Journal of Climate, 19(12): 2743–2762, doi: 10.1175/JCLI3728.1

Mantua N J, Hare S R, Zhang Yuan, et al. 1997. A pacific interdecadal climate oscillation with impacts on salmon production. Bulletin of the American Meteorological Society, 78(6): 1069–1080, doi: 10.1175/1520-0477(1997)078<1069:APICOW>2.0.CO;2

Monin A S, Yaglom A M, Lumley J L. 1971. Statistical Fluid Mechanics: Mechanics of Turbulence. Cambridge, MA, USA: MIT Press

Namias J, Cayan D R. 1981. Large-scale air-sea interactions and short-period climatic fluctuatioins. Science, 214(4523): 869–876, doi: 10.1126/science.214.4523.869

Nonaka M, Xie Shangping. 2003. Covariations of sea surface temperature and wind over the Kuroshio and its extension: evidence for ocean-to-atmosphere feedback. Journal of Climate, 16(9): 1404–1413, doi: 10.1175/1520-0442(2003)16<1404:COSSTA>2.0.CO;2

Okumura Y, Xie Shangping, Numaguti A, et al. 2001. Tropical Atlantic air-sea interaction and its influence on the NAO. Geophysical Research Letter, 28(8): 1507–1510, doi: 10.1029/2000GL012565

O'Neill L W. 2012. Wind speed and stability effects on coupling between surface wind stress and SST observed from buoys and satellite. Journal of Climate, 25(5): 1544–1569, doi: 10.1175/JCLI-D-11-00121.1

O'Neill L W, Chelton D B, Esbensen S K. 2003. Observations of SST-induced perturbations of the wind stress field over the Southern Ocean on seasonal timescales. Journal of Climate, 16(14): 2340–2354, doi: 10.1175/2780.1

O'Neill L W, Chelton D B, Esbensen S K, et al. 2005. High-resolution satellite measurements of the atmospheric boundary layer response to SST variations along the Agulhas Return Current. Journal of Climate, 18(14): 2706–2723, doi: 10.1175/JCLI3415.1

O'Neill L W, Chelton D B, Esbensen S K. 2010. The effects of SST-induced surface wind speed and direction gradients on midlatitude surface vorticity and divergence. Journal of Climate, 23(2): 255–281, doi: 10.1175/2009JCLI2613.1

Park K A, Cornillon P C. 2002. Stability-induced modification of sea surface winds over Gulf Stream rings. Geophysical Research Letter, 29(24): 64-1–64-4

Park K A, Cornillon P C, Codiga D L. 2006. Modification of surface winds near ocean fronts: effects of Gulf Stream rings on scatterometer (QuikSCAT, NSCAT) wind observations. Journal of Geophysical Research: Oceans, 111(C3): C03021

Pezzi L P, Souza R B, Dourado M S, et al. 2005. Ocean-atmosphere in situ observations at the Brazil-Malvinas Confluence region. Geophysical Research Letter, 32(22): L22603

Small R J, deSzoeke S P, Xie S P, et al. 2008. Air–sea interaction over ocean fronts and eddies. Dynamics of Atmospheres and Oceans, 45(3–4): 274–319

Small R J, Xie Shangping, Wang Yuqing. 2003. Numerical simulation of atmospheric response to Pacific tropical instability waves. Journal of Climate, 16(22): 3723–3741, doi: 10.1175/1520-0442(2003)016<3723:NSOART>2.0.CO;2

Song Qingtao, Chelton D B, Esbensen S K, et al. 2009. Coupling between sea surface temperature and low-level winds in mesoscale numerical models. Journal of Climate, 22(1): 146–164, doi: 10.1175/2008JCLI2488.1

Tokinaga H, Tanimoto Y, Xie Shangping. 2005. SST-induced surface wind variations over the Brazil-Malvinas Confluence: satellite and in situ observations. Journal of Climate, 18(17): 3470–3482, doi: 10.1175/JCLI3485.1

Vecchi G A, Xie Shangping, Fischer A S. 2004. Ocean-atmosphere covariability in the western Arabian Sea. Journal of Climate, 17(6): 1213–1224, doi: 10.1175/1520-0442(2004)017<1213:OCITWA>2.0.CO;2

Wallace J M, Smith C, Jiang Quanrong. 1990. Spatial patterns of atmosphere-ocean interaction in the northern winter. Journal of Climate, 3(9): 990–998, doi: 10.1175/1520-0442(1990)003<0990:SPOAOI>2.0.CO;2

Wang Yunhua, Zhang Yanmin, Chen Haihua, et al. 2014. Effects of atmospheric stability and wind fetch on microwave sea echoes. IEEE Transactions on Geoscience and Remote Sensing, 52(2): 929–935, doi: 10.1109/TGRS.2013.2245673

Wu Jin. 1980. Wind-stress coefficients over sea surface near neutral conditions—a revisit. Journal of Physical Oceanography, 10(5): 727–740, doi: 10.1175/1520-0485(1980)010<0727:WSCOSS>2.0.CO;2

Xie Shangping. 2004. Satellite observations of cool ocean-atmosphere interaction. Bulletin of the American Meteorological Society, 85(2): 195–208, doi: 10.1175/BAMS-85-2-195

Xie Shangping, Ishiwatari M, Hashizume H, et al. 1998. Coupled ocean-atmospheric waves on the equatorial front. Geophysical Research Letter, 25(20): 3863–3866, doi: 10.1029/1998GL900014

Xu Haiming, Tokinaga H, Xie Shangping. 2010. Atmospheric effects of the Kuroshio large meander during 2004–05. Journal of Climate, 23(17): 4704–4715, doi: 10.1175/2010JCLI3267.1